Available online at www.sciencedirect.com
SCIENCE DIRECT®
Journal of Solid State Chemistry 176 (2003) 88–96
JOURNAL OF SOLID STATE CHEMISTRY
http://elsevier.com/locate/jssc

Crystal and magnetic structures of $Sr_4MMn_2O_9$ (M= Cu or Zn)

Caroline A. Moore and Peter D. Battle*

Inorganic Chemistry Laboratory, Oxford University, South Parks Road, Oxford OX1 3QR, UK

Received 24 March 2003; received in revised form 6 June 2003; accepted 15 June 2003

Abstract

The crystal and magnetic structures of $Sr_4MMn_2O_9$ (M = Cu, Zn) have been refined from neutron powder diffraction data. These trigonal compounds (space group $P321$, $a = 9.5918(1)$, $c = 7.8114(1)$ Å (Cu); $a = 9.5894(1)$, $c = 7.5039(1)$ Å (Zn)) are $n = 3$ members of the series $A_{3n+3}M_nB_{n+3}O_{6n+9}$, with each unit cell containing three offset [001] polyhedral chains, each of which ideally contains a 1:1 ratio of B_2O_9 units and MO_6 trigonal prisms. In fact anti-site disorder between Mn and M is observed, and for M= Cu the cations are disordered off the center of the prism towards a rectangular face. Both compositions show 3D antiferromagnetic order at 1.6 K, with an ordered magnetic moment of 1.91(6) (M= Cu) or 1.8(1) (M= Zn) μ_B per Mn. No ordered magnetic moment was detected on the trigonal prismatic site in either compound, consistent with the observed temperature dependence of the magnetic susceptibility.

1. Introduction

In recent years the family of compounds represented by the formula $A_{3n+3}M_nB_{n+3}O_{6n+9}$ has been the focus of much attention [1]. The trigonal crystal structures of these materials contain parallel chains, each made up of the same periodic sequence of face-sharing MO_6 and BO_6 polyhedra, with the coordination around M being trigonal prismatic and that around B being octahedral; the sequence of octahedra and prisms within each chain is determined by the value of n. The chains are spaced apart by the remaining cations, A^{2+}, which are typically Ca, Sr or Ba. The presence of cation chains in the crystal structure lead to these materials being used as model compounds in the study of one-dimensional (1D) electronic behavior, with the $n = \infty$ phases A_3MBO_6, in which the chains contain alternating MO_6 and BO_6 units, receiving most attention [2–7]. However, the 1D description of the structure is not entirely valid [8] with some compounds, for example A_3MRuO_6 (A = Ca, Sr; M= Na, Li), showing 3D long-range anti-ferromagnetic order at temperatures as high as 100 K [9,10]. Other $n = \infty$ phases, particularly those containing transition–metal cations on both the prismatic and the octahedral sites, show more complex behavior. For example, several studies [11–14] of $Ca_3Co_2O_6$ ($M = B$= Co) have culminated in the identification [15] of intrachain and interchain ordering temperatures of 24 and 12 K, respectively. The complex behavior can be ascribed in part to the presence of frustration in the magnetically concentrated materials, although this effect can be eliminated by a structural distortion in phases containing the Jahn–Teller active Cu^{2+} species, for example $Ca_{3.1}Cu_{0.9}RuO_6$ [16]. Long-range 3D magnetic order has also been confirmed by neutron diffraction in the cases of Ca_3MMnO_6 (M= Ni, Zn) [17]. However, in some cases [3,18] neutron diffraction experiments have failed to detect magnetic Bragg scattering from samples which clearly show a phase transition in the temperature dependence of their magnetic susceptibility, thus suggesting that a 3D ordered ground state is not always achieved. As implied above, the majority of the research into the electronic properties of the $A_{3n+3}M_nB_{n+3}O_{6n+9}$ phases has been concerned with the $n = \infty$ compositions, possibly because compositions with $n \neq \infty$ can adopt incommensurate crystal structures, thus increasing the complexity of the problem. Neutron diffraction has also been used [19,20] to identify 3D magnetic ordering in the $n = 1$ phases $Ba_6MMn_4O_{15}$ (M= Cu, Zn), which contain Mn_4O_{15} tetramers linked through MO_6 prisms, but no such experiment has been reported previously for an $n = 3$ material, $A_4MB_2O_9$, in which B_2O_9 dimers are separated by an MO_6 prism. In this paper we report the synthesis of polycrystalline samples of nominal composition $Sr_4MMn_2O_9$ (M= Cu, Zn) and their

*Corresponding author. Fax: +44-1865-2726-90.
E-mail address: peter.battle@chem.ox.ac.uk (P.D. Battle).

0022-4596/$ - see front matter © 2003 Elsevier Inc. All rights reserved.
doi:10.1016/S0022-4596(03)00351-7

characterization by magnetometry and neutron diffraction, resulting in the identification of a 3D anti-ferromagnetic ground state in the $n = 3$ structure at 1.6 K.

2. Experimental

All attempts to prepare a polycrystalline sample of $Sr_4CuMn_2O_9$ from a stoichiometric mixture of high purity (Alfa Aesar) $SrCO_3$, CuO and MnO_2 resulted in the formation of an incommensurate structure. It was subsequently determined that a commensurate phase of the form $A_4MB_2O_9$ could be prepared from a mixture of starting materials having a ratio Sr:Cu:Mn of 4:1.04:1.92. The precursors were thoroughly ground and heated in an alumina crucible at 1200°C in air for 6 days with intermittent grinding. In order to synthesize $Sr_4ZnMn_2O_9$, a stoichiometric mixture of $SrCO_3$, ZnO and MnO_2 was intimately ground and calcined at 800°C. Pellets were then pressed and the reactants were heated at 1200°C for a total of 6 days with intermittent grinding. The pellets were covered with a powder of the same nominal composition during the heating cycle in order to prevent loss of Zn from the sample.

The progress of the reactions was followed by X-ray powder diffraction, utilizing Cu$K\alpha_1$ radiation. Neutron diffraction studies were performed over the angular range $10 \leqslant 2\theta/^\circ \leqslant 150$ on the instrument D2b at the Institut Laue Langevin in Grenoble, operating at a wavelength of 1.5955 Å; the unit cell parameters derived from Rietveld analysis of the X-ray diffraction pattern of the Cu-containing sample were used to calibrate the wavelength of the neutron beam. The samples were contained in vanadium cans and mounted in a cryostat for the collection of neutron diffraction data at 290 and 1.6 K. Rietveld [21] analyses of these data were carried out using the Fullprof 2000 [22] program package. The background was fitted using a 5th degree polynomial and the peak shape was described by a pseudo-Voigt function. A narrow angular region ($2\theta \sim 43^\circ$) containing a weak Bragg peak from the V can was excluded from the refinements. Magnetic susceptibility measurements were carried out using a Quantum Design SQUID magnetometer. Data were collected as a function of temperature in a field of 100 Oe after cooling in both zero field (ZFC) and in the measuring field (FC). Measurements of magnetization as a function of field were made at 5 K over the range $-50 \leqslant H/kOe \leqslant 50$.

3. Results

In view of the behavior of other members of this structural family, a 4D incommensurate unit cell [23] was initially used in the analysis of the X-ray powder diffraction patterns of both reaction products. The modulation vector of the Cu-containing phase refined to a value of 0.66694(2), very close to the rational value $\frac{2}{3}$ expected in the case of a commensurate material, and that of the Zn analogue refined to a value of 0.66730(2). Both samples are therefore commensurate within the resolution of our neutron diffraction experiments; all the Bragg peaks in both diffraction patterns could be indexed in the 3D space group $P321$. The room temperature crystal structures of both phases were consequently treated as commensurate and refined using the neutron diffraction data. The fact that the sample of nominal composition $Sr_4CuMn_2O_9$ was commensurate proves that the composition can be expressed in the form $A_4MB_2O_9$ [23]. However, the need to move away from the ideal reactant stoichiometry in order to facilitate the synthesis of a commensurate product indicated that the composition of the product might not be $Sr_4CuMn_2O_9$. Fortunately, as a result of the contrast between the neutron scattering lengths of Cu and Mn ($b_{Cu} = 7.6$ fm, $b_{Mn} = -3.87$), neutron diffraction is sensitive to their relative concentration. The Cu:Mn ratio was therefore allowed to vary during the course of our Rietveld analysis, subject to the constraints that all the six-coordinate M and B sites are occupied, that all the M sites have the same composition, and that all the B sites have the same composition. These assumptions, which control the number of variables in the refinement, are chemically reasonable, although not required by the space group symmetry. The composition refined to be $Sr_4Cu_{1.01(1)}Mn_{1.99(1)}O_9$, slightly Mn-rich compared to that expected from the stoichiometry of the reaction mixture, $Sr_4Cu_{1.04}Mn_{1.92}O_9$. Furthermore, it became clear that the atoms on the M sites do not occupy their idealized positions on the 3-fold axes which pass through the centers of the prisms (1b and 2d in the Wyckoff notation), but that they are displaced towards the rectangular faces of the prisms in a disordered manner. The introduction of this disorder allowed us to arrive at a satisfactory description of this complex structure, although it was necessary to impose constraints on the values of some of the isotropic atomic displacement parameters (ADP, B_{iso}) in order to do so. The refined structural parameters and cation distributions are listed in Tables 1 and 2, bond lengths in Table 3 and bond angles in Table 4. The observed and calculated diffraction patterns are shown in Fig. 1, and the structure is drawn in Fig. 2. At the time of these experiments the diffractometer counter angle was subject to a zeropoint error of $\sim 1^\circ$ and this is reflected in the position of the reflection markers in the relevant figures. In the case of the Zn phase, the refinements converged without the introduction of

Table 1
Structural parameters of $Sr_4MMn_2O_9$ (M = Cu, Zn) at 290 and 1.6 K

	M = Cu		M = Zn	
	290 K	1.6 K	290 K	1.6 K
$a = b$ (Å)	9.5918(1)[a]	9.5699(1)	9.5894(1)	9.5679(1)
c (Å)	7.8114(1)[a]	7.8007(1)	7.5039(1)	7.7851(1)
V (Å^3)	622.39(2)	618.705(8)	621.476(9)	617.201(8)
Sr1 (x, y, z)				
x	0.025(1)	0.0251(8)	0.0242(1)	0.0248(8)
y	0.6897(9)	0.6899(7)	0.6896(8)	0.6910(7)
z	0.248(1)	0.2488(9)	0.249(1)	0.2483(9)
Sr2 (x, 0, $\frac{1}{2}$)				
x	0.358(1)	0.357(1)	0.359(1)	0.358(1)
Sr3 (x, 0, 0)				
x	0.324(1)	0.325(1)	0.324(1)	0.3236(9)
B_{iso} (Å^2)	0.64(3)	0.34(3)	0.76(3)	0.36(3)
$M1$ (x, 0, $\frac{1}{2}$)[b]				
x	0.940(3)	0.942(3)	0	0
$M2$ (x, y, z)[c]				
x	0.382(2)	0.385(2)	1/3	1/3
y	0.661(2)	0.664(2)	2/3	2/3
z	0.750(3)	0.750(2)	0.750(3	0.751(2)
B_{iso}(Å^2)	0.2(2)	0	0.6(2)	0
Mn1 (0, 0, z)				
z	0.159(4)	0.157(4)	0.160(4)	0.160(4)
Mn2 (*1/3,2/3*, z)				
z	0.089(3)	0.087(3)	0.086(4)	0.089(3)
Mn3 (*1/3,2/3*, z)				
z	0.404(3)	0.400(4)	0.402(4)	0.399(3)
B_{iso} (Å^2)	0	0	0	0
μ_{xy}/μ_B	—	1.91(6)	—	1.8(1)
O1 (x, y, z)				
x	0.483(1)	0.484(1)	0.481(1)	0.484(1)
y	0.657(1)	0.656(1)	0.654(1)	0.656(1)
z	0.236(1)	0.235(1)	0.235(1)	0.236(1)
O2 (x, y, z)				
x	0.660(2)	0.679(2)	0.679(1)	0.681(1)
y	0.179(1)	0.180(1)	0.179(1)	0.181(1)
z	0.465(2)	0.465(1)	0.462(1)	0.464(1)
O3 (*x, 0, 0*)				
x	0.843(2)	0.843(2)	0.845(2)	0.847(1)
O4 (x, y, z)				
x	0.678(1)	0.678(1)	0.681(1)	0.6812(9)
y	0.184(1)	0.185(1)	0.184(1)	0.1831(9)
z	0.064(1)	0.066(1)	0.061(1)	0.062(1)
O5 (x, y, z)				
x	0.990(1)	0.991(1)	0.990(1)	0.993(1)
y	0.156(2)	0.991(1)	0.155(1)	0.156(1)
z	0.294(2)	0.159(1)	0.300(1)	0.301(1)
B_{iso}(Å^2)				
O1, O3	0.68(6)	0.41(5)	0.71(6)	0.65(5)
O2, O4, O5	1.32(5)	1.04(4)	0.96(4)	0.54(4)
R_{wp}(%)	6.27	6.06	7.15	7.44
χ^2	1.80	2.18	3.86	4.62

Space group $P321$.
[a] Lattice parameters determined from X-ray data.
[b] Center of prism lies on the Wyckoff 1b site at (0, 0, 1/2); for M = Cu the atoms disorder onto the Wyckoff 3f (x, 0, 1/2) site with a fractional occupancy of 1/3.
[c] Center of prism lies on the 2d site at (1/3,2/3, z); atoms disorder onto 6g(x, y, z).

Table 2
Cation distribution in $Sr_4MMn_2O_9$ (M = Cu, Zn)

	M = Cu	M = Zn
Trigonal prisms M:Mn	0.921(9):0.081(9)	0.870(6):0.129(6)
Octahedra M:Mn	0.045(3):0.954(3)	0.039(3):0.960(3)

Table 3
Bond lengths (Å) $Sr_4MMn_2O_9$ (M = Cu, Zn)

	M = Cu		M = Zn	
	290 K	1.6 K	290 K	1.6 K
M1–O5	2.08(1) × 2	2.10(1) × 2	2.19(1) × 6	2.17(1) × 6
	2.12(1) × 2	2.13(1) × 2		
	2.66(3) × 2	2.65(2) × 2		
M2–O2	2.15(2)	2.14(2)	2.27(2) × 3	2.27(2) × 3
	2.17(3)	2.16(2)		
	2.64(3)	2.64(2)		
M2–O4	1.95(2)	1.93(2)	2.10(2) × 3	2.10(1) × 3
	1.98(2)	1.95(2)		
	2.46(3)	2.45(2)		
Mn1–O3	1.95(2) × 3	1.94(2) × 3	1.94(2) × 3	1.92(2) × 3
Mn1–O5	1.87(2) × 3	1.89(2) × 3	1.88(2) × 3	1.88(2) × 3
Mn2–O1	1.88(2) × 3	1.89(2) × 3	1.88(2) × 3	1.88(2) × 3
Mn2–O4	1.91(2) × 3	1.89(2) × 3	1.90(2) × 3	1.91(2) × 3
Mn3–O1	1.97(2) × 3	1.97(2) × 3	1.98(2) × 3	1.96(2) × 3
Mn3–O2	1.86(2) × 3	1.86(2) × 3	1.87(2) × 3	1.87(2) × 3
Mn1–Mn1	2.45(4)	2.45(5)	2.50(5)	2.49(4)
Mn2–Mn3	2.47(4)	2.44(4)	2.47(4)	2.42(4)
M1–Mn1	2.73(3)	2.73(3)	2.65(3)	2.65(3)
M2–Mn2	2.70(3)	2.68(3)	2.62(3)	2.63(3)
M2–Mn3	2.76(4)	2.76(4)	2.72(3)	2.74(3)

displacive disorder at the prismatic sites. However, there was evidence of occupational disorder between the M and B sites (b_{Zn} = 5.7 fm), with the composition refining to be $Sr_4Zn_{0.95(1)}Mn_{2.05(1)}O_9$, again Mn-rich compared to the reaction mixture. The results of these refinements are included in Tables 1–4, and the fitted diffraction pattern is shown in Fig. 3.

Additional Bragg scattering was observed in some reflections at low scattering angles in the neutron diffraction patterns collected at 1.6 K; the changes on cooling were essentially the same for both samples. This additional scattering was assumed to be magnetic in origin, and it was best accounted for by the collinear magnetic structure drawn in Fig. 4; the magnetic unit cell and the structural unit cell are the same size. The magnetic moments of the Mn cations within the dimers align in the xy plane, but the atomic moments at the prismatic sites do not show long-range magnetic order. There were no significant changes in the crystal structure on cooling and refinements proceeded smoothly in space group $P321$; the cation distributions determined at

Table 4
Bond angles (degrees) in $Sr_4MMn_2O_9$ (M= Cu, Zn)

	O–M–O	M=Cu		M=Zn	
		290 K	1.6 K	290 K	1.6 K
Mn1	O3–Mn1–O3	84(1) × 3	84(1) × 3	83(1) × 3	83(1) × 3
	O3–Mn1–O5	91(1) × 3	90(1) × 3	92(1) × 3	93(1) × 3
		94(1) × 3	94(1) × 3	95(1) × 3	95(1) × 3
		174(2) × 3	175(1) × 3	175(1) × 3	175(1) × 3
	O5–Mn1–O5	91(1) × 3	91(1) × 3	90(1) × 3	89(1) × 3
Mn2	O1–Mn2–O1	87(1) × 3	86(1) × 3	86(1) × 3	87(1) × 3
	O1–Mn2–O4	179(1) × 3	179(1) × 3	179(1) × 3	179(1) × 3
		94(1) × 3	94(1) × 3	93(1) × 3	92.8(9) × 3
		94(1) × 3	94(1) × 3	94(1) × 3	94.1(9) × 3
	O4–Mn2–O4	85(1) × 3	85(1) × 3	87(1) × 3	86.3(9) × 3
Mn3	O1–Mn3–O1	82(1) × 3	82(1) × 3	81(1) × 3	83(1) × 3
	O1–Mn3–O2	93(1) × 3	93(1) × 3	94(1) × 3	93(1) × 3
		93(1) × 3	93(1) × 3	94(1) × 3	94(1) × 3
		172(2) × 3	174(1) × 3	173(1) × 3	174(1) × 3
	O2–Mn3–O2	92(1) × 3	91(1) × 3	91(1) × 3	91(1) × 3
*M*1	O5–*M*1–O5	79.0(8) × 2	79.7(6) × 2	74.7(7) × 6	74.9(5) × 3
		100.1(8) × 2	99.1(7) × 2	91.2(7) × 3	90.9(6) × 3
		165(1)	164.0(9)	135.2(8) × 3	136.0(7) × 3
		173(1)	170.9(9)	142.9(9) × 3	141.8(8) × 3
		67.4(8) × 2	68.3(7) × 2		
		67.0(7) × 2	67.9(7) × 2		
		126(1) × 2	126.2(9) × 2		
		119(1) × 2	120.2(8) × 2		
		74.6(9)	74.6(8)		
*M*2	O2–*M*2–O2	67(1)	66.6(9)	72.4(9) × 3	71.6(7) × 3
		67(1)	66.4(9)		
		76(1)	76.3(9)		
	O2–*M*2–O4	75.8(8)	75.4(8)	91.3(8) × 3	91.3(7) × 3
		124(1)	125(1)	139(1) × 3	139.0(8) × 3
		126(1)	124(1)	139(1) × 3	138.9(8) × 3
		124(1)	124(1)		
		98(1)	100(1)		
		165(1)	166(1)		
		124(1)	123(1)		
		165(1)	166(1)		
		99(1)	98.4(9)		
	O4–*M*2–O4	70(1)	70.1(9)	76.6(8) × 3	77.3(7) × 3
		70(1)	69.9(9)		
		82(1)	82.3(9)		

290 K were assumed to be unchanged at 1.6 K. The results of these refinements, in which the ordered magnetic moment at the octahedral site was a variable, are included in Tables 1, 3 and 4, and the fitted diffraction patterns are shown in Figs. 5 and 6.

The molar magnetic susceptibilities of $Sr_4CuMn_2O_9$ and $Sr_4ZnMn_2O_9$ (nominal compositions will be used throughout this paper) are shown in Figs. 7 and 8, respectively. They show a relatively weak temperature dependence (incompatible with a Curie–Weiss law) in the range $50 < T/K < 300$, although there is clear evidence of a broad maximum centered on 120 K in the susceptibility of $Sr_4ZnMn_2O_9$. and a decrease in the gradient of $\chi(T)$ for $Sr_4CuMn_2O_9$ at approximately the same temperature. The susceptibility of both materials increases below ~25 K, with some hysteresis apparent between the FC and ZFC data; this is emphasized by the displaced $M(H)$ hysteresis loop (Fig. 7(b)) recorded for $Sr_4CuMn_2O_9$.

4. Discussion

The structural chemistry of $Sr_4CuMn_2O_9$ is relatively complex. The sample described above was commensurate, with a refined composition very close to the ideal stoichiometry, even though the reactant mixture was made Cu-rich. No other phases were detected in the X-ray or neutron diffraction patterns, suggesting that any crystalline impurity was only present at a level of ~1%. Our failure to prepare a commensurate sample from a reaction mixture having the ideal stoichiometry is consistent with the recent work of Bazuev et al. and El Abed et al. [24,25], who have described the preparation and properties of a polycrystalline incommensurate phase which was synthesized from a 4:1:2 Sr:Cu:Mn reaction mixture. The detection and identification of a second phase, perhaps of low crystallinity, in these samples are issues that remain to be addressed in the future. Our sample of $Sr_4ZnMn_2O_9$ was also found to be Mn-rich relative to the mixture of starting materials, and it is likely that a ~1% minority phase is also present in this sample. The presence of anti-site defects and, in the case of $Sr_4CuMn_2O_9$, displacive disorder, necessitated the use of certain assumptions in refining the crystal structures. As is apparent in Table 1, we imposed constraints on some ADPs and, in the case of $Sr_4CuMn_2O_9$, we assumed that the small number of Mn cations which occupy prismatic sites show the same displacive disorder as the Cu cations which are located on the majority of these sites. The latter assumption was made following a number of trial refinements. We regard it as questionable but necessary in view of the complexity of the structure and the limitations of the data. El Abed et al. [26] have recently performed single crystal X-ray diffraction experiments on a flux-grown sample of composition $Sr_4Cu_{0.91}Mn_{2.09}O_9$ and introduced stacking faults (with a density of 14%) in the sequence of octahedra and prisms along just one of the two crystallographically distinct [001] chains in order to model the structure; they did not explicitly introduce anti-site defects. However, they recognized that there should be a disordered Cu position around each Mn2 site which is adjacent to a stacking fault, although they were unable to refine a model including this extra site. Thus both ourselves and El Abed et al. have been forced by the delocalized scattering density to compromise, albeit in different ways, in order to produce a model which can be refined. The model described in Table 1 gives a better account of our neutron data than the

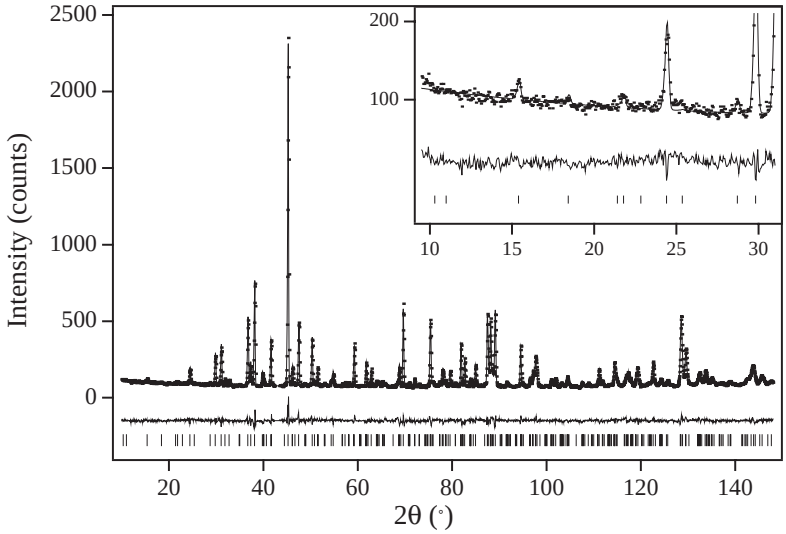

Fig. 1. Observed (.), calculated (-) and difference neutron powder diffraction patterns of $Sr_4CuMn_2O_9$ at room temperature. Reflection positions are marked by vertical bars.

model derived from the X-ray study, thus suggesting that synthesis conditions and small changes in composition can have a marked effect on the details of the crystal structure. $Sr_4ZnMn_2O_9$ has also been prepared before [27], but although the microstructure was studied in detail by electron microscopy, no attempt was made to analyze the structure by X-ray or neutron diffraction. However, a study of $Sr_{3.3}Ca_{0.7}CoRh_2O_9$ [28] by X-ray powder diffraction did find evidence for Co/Rh disorder over the octahedral and prismatic sites.

The Mn–Mn distances within the dimers of $Sr_4MMn_2O_9$ are very similar to those which occur within the Mn_4O_{15} groups in $n = 1$ $Ba_6MMn_4O_{15}$ [19]; they are, on average, slightly shorter than that within the Mn_2O_9 dimers of 4*H* $SrMnO_3$ (2.500 Å [29]). The mean octahedral Mn–O distances are 1.91 and 1.90 Å for M= Cu and Zn, respectively (1.89 Å in $SrMnO_3$). As a consequence of the disorder in the structure, the precision of our results is relatively low. It is nevertheless interesting to note that we are unable to detect (Table 3, Fig. 2) any significant difference between the two independent bond lengths around the Mn2 site in either the Cu or the Zn compound. This is surprising because cation–cation repulsions within the dimer would be expected to lengthen the bonds between Mn and the anions (O1) in the shared octahedral face. If the cations in the prismatic sites of $Sr_4CuMn_2O_9$ are assumed to be four-coordinate, then the mean Cu–O bond lengths at these sites are 2.10 and 2.06 Å; the mean bond length at both of the prismatic sites holding six-coordinate Zn in $Sr_4ZnMn_2O_9$ is 2.19 Å. The latter value is in excellent agreement with those reported previously [4,18,30] for $n = \infty$ phases Sr_3ZnBO_6 (B= Rh, Ir, Pt); the former can be compared to the values reported in compounds in which the displacement of the Cu cations occurs in an ordered manner with a concomitant reduction in symmetry. In the case of $Ca_{3.1}Cu_{0.9}RuO_6$ [16] the mean Cu–O distance is 2.01 Å, and short values (2.04, 2.00 and 2.01 Å) have also been reported [31–33] in other ordered compounds. The Cu–O distances in $Sr_4CuMn_2O_9$ thus appear to be rather long, although the distances to the next two anions (2.65 Å) are shorter than in the other compounds (>2.70 Å), thus increasing the bond-valence sum about the Cu site; it is not sensible to attempt an accurate calculation of this sum in a disordered material. Furthermore, it is likely that, as suggested by the high value of the ADP at 1.6 K (1.04 $Å^2$), the O2, O4 and O5 sublattices disorder in response to the disorder amongst the prismatic cations; we were not able to model this anion disorder using the available data. We note that the four shortest Cu–O bonds in disordered $n = 1$ $Ba_6CuMn_4O_{15}$ are ~2.12 Å in length.

The magnetic structure illustrated in Fig. 4 involves anti-ferromagnetic coupling of the Mn cations within each dimer; this will be the strongest magnetic interaction in these compounds. The ordered Mn magnetic moments (Table 1) are significantly larger than those measured in the non-collinear spin structures of $n = 1$ $Ba_6MMn_4O_{15}$ (M= Cu, Zn) and $n = 0$ $BaMnO_3$ [34], all of which show the effects of magnetic frustration. In the case of $Sr_4ZnMn_2O_9$ the next-strongest interaction, if we ignore the low concentration of Mn cations in the prismatic sites, will be between Mn cations in neighboring dimers in the same [001] chain, or between Mn cations in neighboring chains; the former would be expected to dominate if the structure is to be considered 1D. In both cases the proposed structure provides the anti-ferromagnetic coupling preferred by d^3 cations; there are no frustrated nearest or next-nearest neighbor interactions in this spin arrangement, and the magnetic ground state of this compound is readily explained. The behavior of $Sr_4CuMn_2O_9$ is less easily accounted for

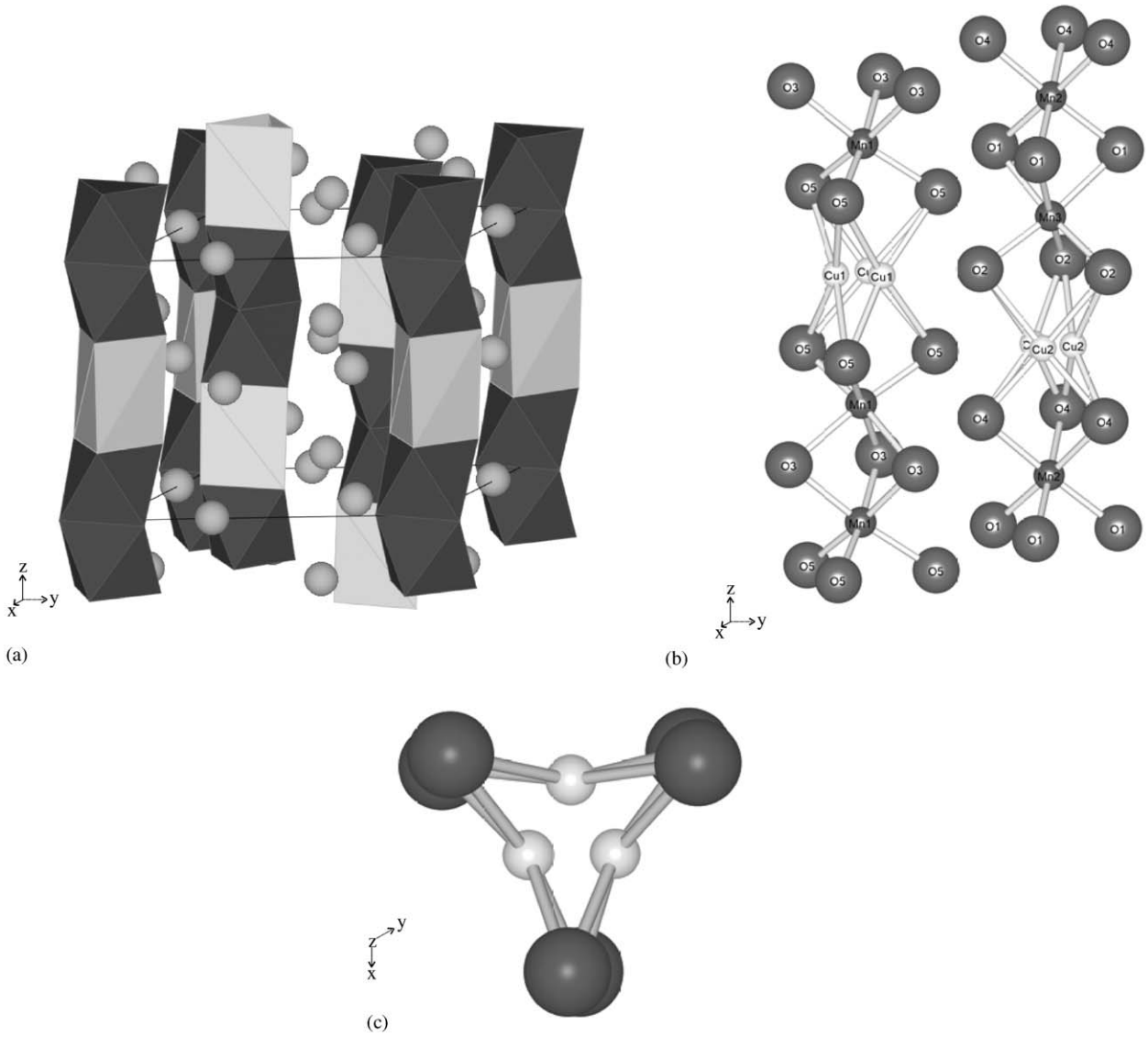

Fig. 2. Crystal structure of $Sr_4CuMn_2O_9$: (a) polyhedral representation, (b) atomic arrangement showing disorder at the prismatic sites; labels identify the majority cation at each site and (c) [001] view showing disorder within the prisms.

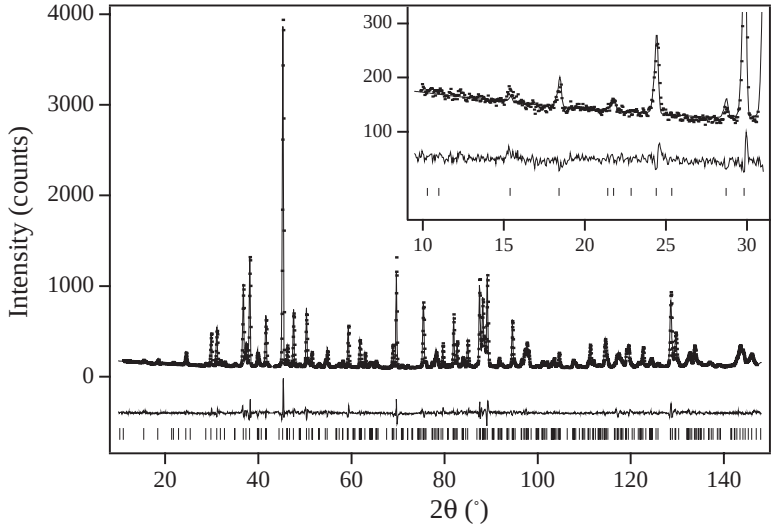

Fig. 3. Observed (.), calculated (-) and difference neutron powder diffraction patterns of $Sr_4ZnMn_2O_9$ at room temperature. Reflection positions are marked by vertical bars.

because there is a high concentration of magnetic cations in the trigonal prisms. However, we have previously shown that the presence of paramagnetic Cu^{2+} cations, displaced in a disordered manner, leads to magnetic frustration among the superexchange pathways of $Ba_6CuMn_4O_{15}$, and results in a paramagnetic contribution from the prismatic sites, with some degree of spin freezing at very low temperatures. The same argument can be used in the case of $Sr_4CuMn_2O_9$. The change in the gradient of the susceptibility of both compounds at $\sim$120 K signals the development of short-range spin ordering within the Mn_2O_9 dimers [24], and the increase in the susceptibility at lower temperatures can be attributed to the paramagnetism of the Cu^{2+} cations $Sr_4CuMn_2O_9$ or to the few Mn^{4+} cations which occupy prismatic sites in $Sr_4ZnMn_2O_9$. It is not clear from our data whether or not extensive 1D inter-dimer coupling occurs above the Néel temperature. The hysteresis observed below $\sim$20 K signals the onset of spin freezing at the prismatic sites, although the details of the magnetic behavior will be further complicated by the existence, as a consequence of the site disorder, of some $MnZnO_9$ and $MnCuO_9$ dimers. The spin pairing in the dimers at relatively high temperatures considerably reduces the magnetization of the samples before long-range order is established, and consequently there is no marked drop in the susceptibilities to indicate the value of the Néel temperature. These are systems which progress from a state of short-range magnetic order to long-range order, with some spins which are not coupled to the magnetic backbone possibly freezing at lower temperatures. We have previously given examples of systems in which the true 3D ordering temperature can only be determined reliably [20] by recording neutron diffraction patterns as a function of temperature. Previous magnetometry experiments on $Sr_4ZnMn_2O_9$ and $Sr_4CuMn_2O_9$ [25,27] have claimed to identify transitions at 7 K, although we do not find the data convincing, particularly in the former case.

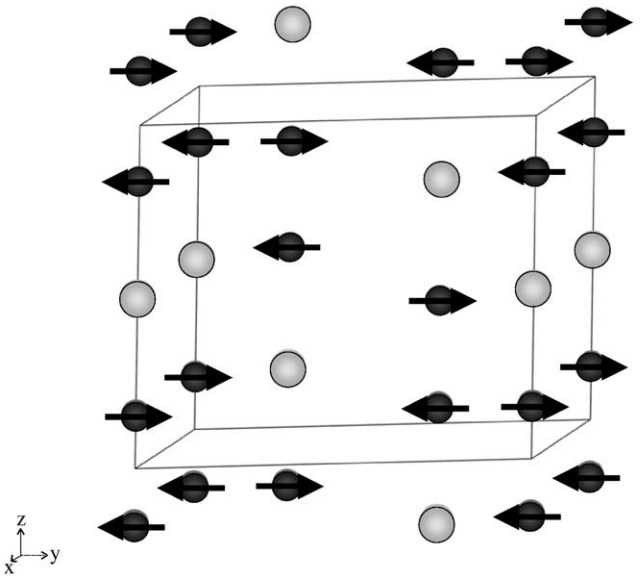

Fig. 4. Magnetic structure of $Sr_4CuMn_2O_9$ and $Sr_4ZnMn_2O_9$: spin direction at octahedral sites shown by arrows, lighter circles represent prismatic sites.

To conclude, our model for the structure of $Sr_4CuMn_2O_9$ has a number of features in common with that proposed previously [26], including the existence of displacive disorder on the prismatic sites. However, our data, which have the advantage of being collected using neutron rather than X-ray diffraction, but the disadvantage of being collected from a powder sample rather than a single crystal, lead to a different description of the disorder. As a consequence of the disorder, the bond

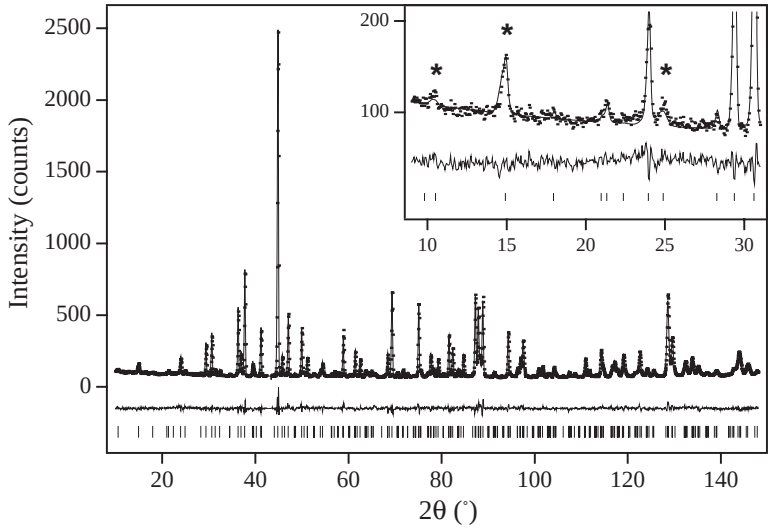

Fig. 5. Observed (.), calculated (-) and difference neutron powder diffraction patterns of $Sr_4CuMn_2O_9$ at 1.6 K. Reflection positions are marked by vertical bars. The strongest magnetic reflections are marked (*).

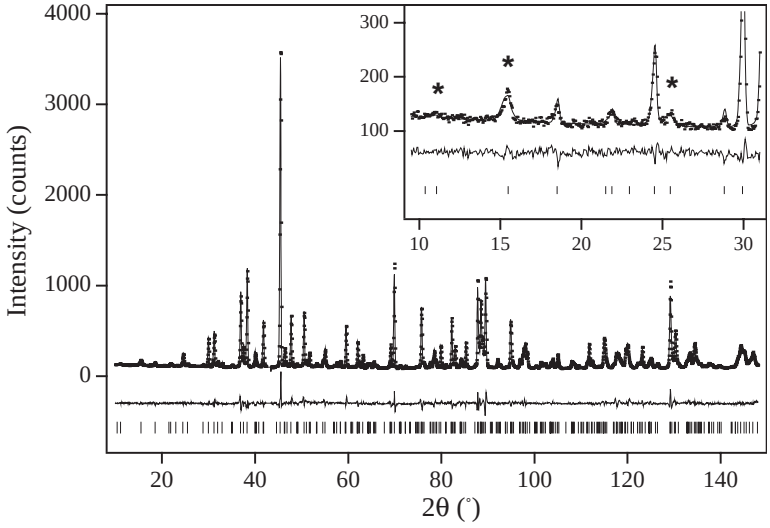

Fig. 6. Observed (.), calculated (-) and difference neutron powder diffraction patterns of $Sr_4ZnMn_2O_9$ at 1.6 K. Reflection positions are marked by vertical bars. The strongest magnetic reflections are marked (*).

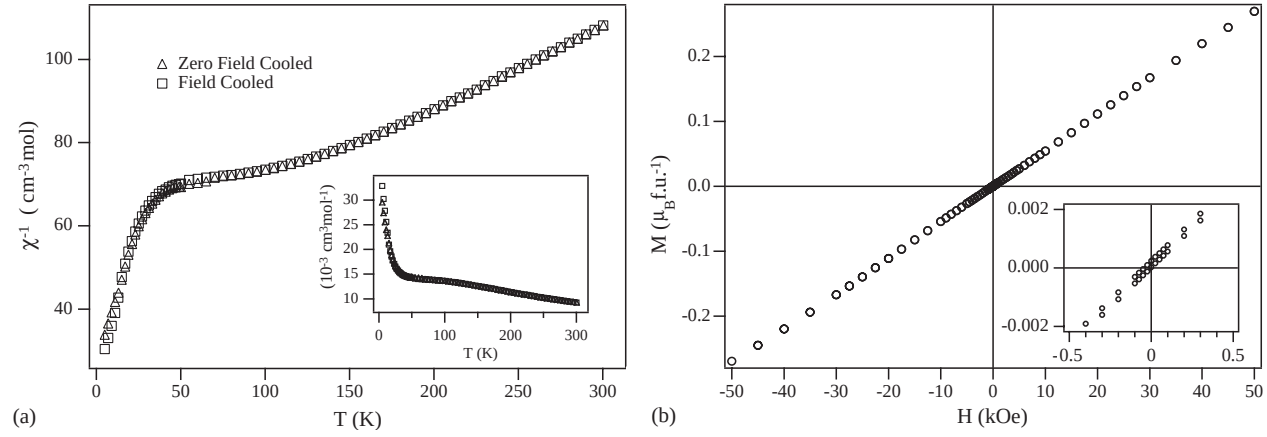

Fig. 7. Temperature dependence of the inverse molar magnetic susceptibility of $Sr_4CuMn_2O_9$, with the molar susceptibility inset; (b) magnetization per formula unit of $Sr_4CuMn_2O_9$ as a function of applied field at 5 K.

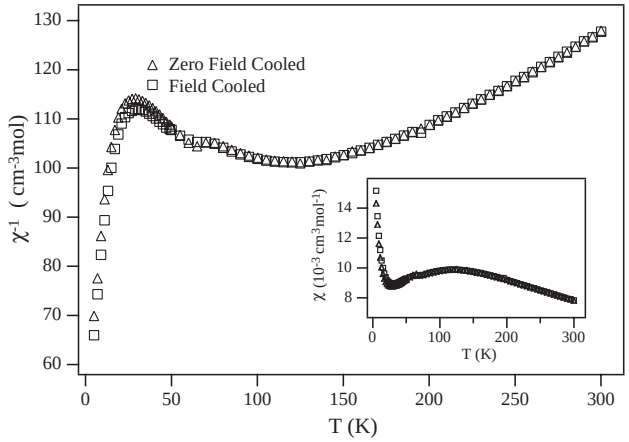

Fig. 8. Temperature dependence of the inverse molar magnetic susceptibility of $Sr_4ZnMn_2O_9$, with the molar susceptibility inset.

distances derived in our study are of relatively low precision. The interpretation given above of our magnetic susceptibility measurements on $Sr_4CuMn_2O_9$ is consistent with our previous study of $Ba_6CuMn_4O_{15}$ and $Ba_6ZnMn_4O_{15}$. It is also largely consistent with the accounts of incommensurate $Sr_4CuMn_2O_9$ given recently [24,25] and with previous descriptions of the magnetic properties of $Sr_{3.3}Ca_{0.7}CoRh_2O_9$, which was described as adopting a partially ordered magnetic state [28], and $Sr_4NiMn_2O_9$ [35] in which the Mn sublattice was assumed to show anti-ferromagnetic order whilst the disordered, prismatically coordinated Ni^{2+} cations were assumed to be 80% diamagnetic (if they lie in a rectangular face of the prism) and 20% paramagnetic (if they remain in the center of the prism). Similarly, our measurements of the magnetic susceptibility of $Sr_4ZnMn_2O_9$ agree well with those

reported previously [27]. Our study is the first to describe in detail the anti-ferromagnetic structure adopted by these $n = 3$ phases at low temperatures; the interpretation of the magnetic scattering is essentially independent of the way in which the structural disorder is modeled. The prismatic sites are magnetically dilute in $Sr_4ZnMn_2O_9$ and disordered in $Sr_4CuMn_2O_9$. Thus, albeit for different reasons, in both compounds only the octahedral sites are involved in the long-range magnetic ordering, no frustration is present, and a collinear spin structure is adopted at low temperatures.

Acknowledgments

We are grateful to EPSRC for funding, and to T. Hansen for experimental assistance at ILL Grenoble.

References

[1] K.E. Stitzer, J. Darriet, H.-C. zur Loye, Curr. Opin. Solid State Mater. Sci. 5 (2001) 535.
[2] T.N. Nguyen, D.M. Giaquinta, H.-C. zur Loye, Chem. Mater. 6 (1994) 1642.
[3] T.N. Nguyen, H.-C. zur Loye, J. Solid State Chem. 117 (1995) 300.
[4] C. Lampe-Önnerud, H.-C. zur Loye, Inorg. Chem. 35 (1996) 2155.
[5] J.F. Vente, J.K. Lear, P.D. Battle, J. Mater. Chem. 5 (1995) 1785.
[6] T.N. Nguyen, P.A. Lee, H.-C. zur Loye, Science 271 (1996) 489.
[7] H. Kageyama, K. Yoshimura, K. Kosuge, J. Solid State Chem. 140 (1998) 14.
[8] S.H. Irons, T.D. Sangrey, K.M. Beauchamp, M.D. Smith, H.C. zur Loye, Phys. Rev. B 61 (2000) 11594.
[9] P.D. Battle, G.R. Blake, J.C. Burley, E.J. Cussen, J. Sloan, J.F. Vente, J. Darriet, F. Weill, MRS Symp. Proc. 547 (1999) 45.
[10] J. Darriet, F. Grasset, P.D. Battle, Mater. Res. Bull. 32 (1997) 139.
[11] H. Kageyama, S. Kawasaki, K. Mibu, M. Takano, K. Yoshimura, K. Kosuge, Phys. Rev. Lett. 79 (1997) 3258.
[12] H. Kageyama, K. Yoshimura, K. Kosuge, H. Mitamura, T. Goto, J. Phys. Soc. Japan 66 (1997) 1607.
[13] S. Aasland, H. Fjellvåg, B. Hauback, Solid State Commun. 101 (1997) 187.
[14] H. Fjellvåg, E. Gulbrandsen, S. Aasland, A. Olsen, B.C. Hauback, J. Solid State Chem. 124 (1996) 190.
[15] A. Maignan, C. Michel, A.C. Masset, C. Martin, B. Raveau, Eur. Phys. J. B 15 (2000) 657.
[16] C.A. Moore, E.J. Cussen, P.D. Battle, J. Solid State Chem. 153 (2000) 254.
[17] S. Kawasaki, M. Takano, T. Inami, J. Solid State Chem. 145 (1999) 302.
[18] C. Lampe-Önnerud, M. Sigrist, H.-C. zur Loye, J. Solid State Chem. 127 (1996) 25.
[19] E.J. Cussen, J.F. Vente, P.D. Battle, J. Am. Chem. Soc. 121 (1999) 3958.
[20] P.D. Battle, E.J. Cussen, Mater. Res. Soc. Symp. Proc. 658 (2001) GG2.4.1.
[21] H.M. Rietveld, J. Appl. Crystallogr. 2 (1969) 65.
[22] J. Rodriquez-Caravajal, FULLPROF version 2.10, ILL, 2002, unpublished.
[23] J.M. Perez-Mato, M. Zakhour-Nakhl, F. Weill, J. Darriet, J. Mater. Chem. 9 (1999) 2795.
[24] A. El-Abed, E. Gaudin, H.-C. zur Loye, J. Darriet, Solid State Sci. 5 (2003) 59.
[25] G.V. Bazuev, V.N. Krasil'nikov, D.G. Kellerman, J. Alloys Compd. 352 (2003) 190.
[26] A. El Abed, E. Gaudin, J. Darriet, Acta Crystallogr. C 58 (2002) i138.
[27] M. Hernando, K. Boulahya, M. Parras, J.M. González-Calbet, Eur. J. Inorg. Chem. 2002 (2002) 3190.
[28] M. Hernando, K. Boulahya, M. Parras, A. Varela, J.M. González-Calbet, J.L. Martínez, Chem. Mater. 14 (2002) 4948.
[29] P.D. Battle, T.C. Gibb, C.W. Jones, J. Solid State Chem. 74 (1988) 60.
[30] R.C. Layland, H.C. zur Loye, J. Alloys Compd. 299 (2000) 118.
[31] M. Neubacher, H. Müller-Buschbaum, Z. Anorg. Allg. Chem. 607 (1992) 124.
[32] A. Tomaszewska, H. Müller-Buschbaum, Z. Anorg. Allg. Chem. 619 (1993) 534.
[33] A.P. Wilkinson, A.K. Cheetham, W. Kunnman, Å. Kvick, Eur. J. Solid State Chem. 28 (1991) 453.
[34] E.J. Cussen, P.D. Battle, Chem. Mater. 12 (2000) 831.
[35] A. El Abed, E. Gaudin, S. Lemaux, J. Darriet, Solid State Sci. 3 (2001) 887.